Atmospheric Environment

Impact of Stratospheric Intrusions on Surface Ozone Enhancement in Hong Kong in the Lower Troposphere: Implications for Ozone Control Strategy

--Manuscript Draft--

Manuscript Number:	ATMENV-D-24-00180
Article Type:	Research Paper
Keywords:	Stratospheric intrusion; O3 pollution; emission reduction path; Hong Kong
Abstract:	Understanding the impact of stratospheric intrusion (SI) is crucial for elucidating atmospheric complexities and implications for ozone (O3) control. However, current studies have not focused on the influence of SI on surface O3, thus limiting the effectiveness of control strategies. This study delves into an SI event that occurred from March 5 to 12, 2022, employing a comprehensive integration of the Weather Research and Forecasting model coupled with Chemistry and multi-reanalysis data. A distinctive spatial–temporal O3 distribution in Hong Kong elevated stratospheric O3 in the lower troposphere, despite the absence of an SI in the upper troposphere. This study employed a comprehensive methodology, integrating the use of a box model to estimate the stratosphere–troposphere exchange (STE) O3 flux, integrated process rate (IPR) analysis to quantify the contributions from individual physical and chemical processes, and tracer methods to detect stratospheric O3. During the deep SI episode, the STE flux peaked at −81.33×10-8 kg·m-2·s-1, surpassing the monthly average by 15.2-fold. The IPR results indicate that vertical transport within the 0–16 km range contributes between 18.4 and 39.0 ppbv·hr-1 during the SI event, whereas horizontal advection shows a negative contribution. Stratospheric O3 tagging revealed that SI contributes 15.5–31.3 ppb (29.6–50.2%, respectively, of surface O3) when stratospheric O3 mixes down. Five emission reduction paths were designed in response to the negative impacts of SI. The “anthropogenic VOC (AVOC) only” path was the most efficient; however, when SI contributed 31 ppb on March 9, the “NOx only” path required a 69% reduction, while the “AVOC only” path required an 85% reduction for efficiency. This research not only elucidates the complex interplay between SI and surface O3 concentrations but also emphasizes the significance of refining existing emission reduction paths.

Graphical Abstract

Click here to access/download;Graphical Abstract (for review);graphic abstract.docx

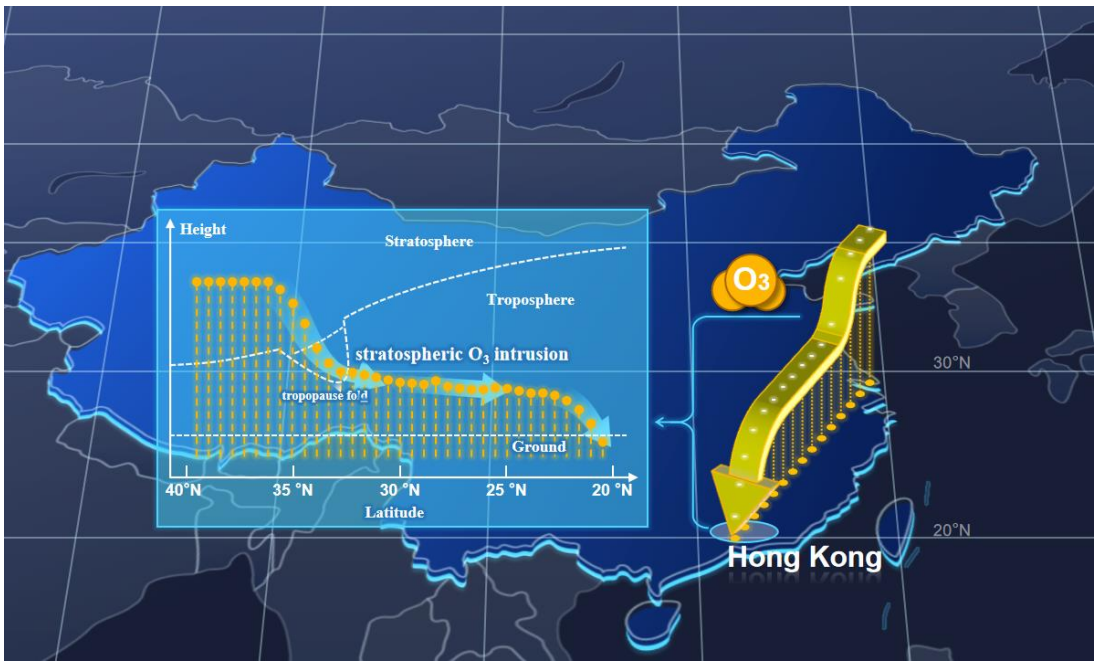

- A distinctive stratospheric intrusion (SI) event in Hong Kong was evidenced
- Tagging method revealed that SI contributes 15.5–31.3 ppb to surface O_3 enhancement
- It is crucial to offset the adverse effects of SI on emission reduction strategies
- The optimal emission reduction path needs to be adjusted as the impact of SIs changes

Impact of Stratospheric Intrusions on Surface Ozone Enhancement in Hong Kong in the Lower Troposphere: Implications for Ozone Control Strategy

Kaihui Zhao[a,b], Yuheng Chen[a], Puyu Lian[c], Wenguang Li[d], Fangyuan Yang[e], Xiufang Zhang[f], Ruowen Yang[a,*]

[a] *Yunnan Key Laboratory of Meteorological Disasters and Climate Resources in the Greater Mekong Subregion, Yunnan University, Kunming, 650091, China*

[b] *Xianyang Intelligence Meteorological Engineering Technology Research Center, 712021, China*

[c] *School of Environment and Energy, South China University of Technology, Guangzhou 510006, China*

[d] *School of Management, Wuhan University of Technology, 430070, China*

[e] *Kunming Meteorological Bureau, Kunming 650000, China*

[f] *Yunnan Meteorological Service Center, Kunming 650000, China*

Corresponding author: Ruowen Yang (yangruowen@ynu.edu.cn)

Abstract

Understanding the impact of stratospheric intrusion (SI) is crucial for elucidating atmospheric complexities and implications for ozone (O_3) control. However, current studies have not focused on the influence of SI on surface O_3, thus limiting the effectiveness of control strategies. This study delves into an SI event that occurred from March 5 to 12, 2022, employing a comprehensive integration of the Weather Research and Forecasting model coupled with Chemistry and multi-reanalysis data. A distinctive

spatial–temporal O_3 distribution in Hong Kong elevated stratospheric O_3 in the lower troposphere, despite the absence of an SI in the upper troposphere. This study employed a comprehensive methodology, integrating the use of a box model to estimate the stratosphere–troposphere exchange (STE) O_3 flux, integrated process rate (IPR) analysis to quantify the contributions from individual physical and chemical processes, and tracer methods to detect stratospheric O_3. During the deep SI episode, the STE flux peaked at -81.33×10^{-8} kg·m^{-2}·s^{-1}, surpassing the monthly average by 15.2-fold. The IPR results indicate that vertical transport within the 0–16 km range contributes between 18.4 and 39.0 ppbv·hr^{-1} during the SI event, whereas horizontal advection shows a negative contribution. Stratospheric O_3 tagging revealed that SI contributes 15.5–31.3 ppb (29.6–50.2%, respectively, of surface O_3) when stratospheric O_3 mixes down. Five emission reduction paths were designed in response to the negative impacts of SI. The "anthropogenic VOC (AVOC) only" path was the most efficient; however, when SI contributed 31 ppb on March 9, the "NOx only" path required a 69% reduction, while the "AVOC only" path required an 85% reduction for efficiency. This research not only elucidates the complex interplay between SI and surface O_3 concentrations but also emphasizes the significance of refining existing emission reduction paths.

Keywords: Stratospheric intrusion; O_3 pollution; Emission reduction path; Hong Kong

1. INTRUDUCTION

Although air pollution in China has significantly improved since the implementation of the Air Pollution Prevention and Control Action Plan in 2013, maintaining ozone (O_3) levels has become an emerging and urgent task for policymakers in China. As a secondary air pollutant, tropospheric O_3 is chiefly produced by photochemical reactions between O_3 precursors, such as nitrogen oxides (NOx) and volatile organic compounds (VOCs), under favorable meteorological conditions (Westervelt et al., 2019; Zhao et al., 2021a; Zhao et al., 2022). Apart from local chemical reactions, stratospheric intrusion

(SI), the largest natural source of O_3, can transport O_3-laden air from the stratosphere downward to the troposphere, thus enhancing surface O_3 concentrations at certain locations.

Extensive observations and numerical simulations have been conducted to investigate the physical mechanisms that drive SI (Holton et al., 1995; Olsen et al., 2000; Stohl et al., 2003). Prior research has identified the dynamic mechanism driving SI at different latitudes, which is attributed to Brewer–Dobson circulation, extratropical cyclones, tropopause folding, wave breaking, and cut-off lows (Li et al., 2015). On a global scale, Brewer–Dobson circulation is believed to be the major process that transports tropospheric air upward into the stratosphere in the tropics and descends into the upper troposphere in the middle and high latitudes (Brewer, 1949; Dobson and Massey, 1956). From a regional perspective, the downwelling branches of the Hadley and Ferrel cells can transport accumulated O_3-enriched air from the upper troposphere downward into the lower troposphere at middle and high latitudes (Lachmy and Harnik, 2014). At low to middle northern hemisphere latitudes, the subtropical jet stream (STJ) has been identified as a key mechanism of SI (Langford, 1999; Zhao et al., 2021b). Subsidence motion associated with the STJ can transport O_3-enriched air down to the lower troposphere. In high-latitude regions, turbulent mixing caused by cut-off low systems can irreversibly mix stratospheric air with the troposphere (Li et al., 2015; Price and Vaughan, 1993). In these studies, the physical mechanisms of SI have been extensively investigated.

As an irregular and uncontrollable natural event, the potential contribution of SI to O_3 has drawn less attention in the past. However, the lack of consideration of its impact would weaken the effectiveness of emission reduction strategies. Therefore, the extent to which SI exacerbates surface O_3 pollution must be addressed. Few studies have attempted to quantify the impact of SI on the tropospheric O_3 budget by calculating the stratosphere–troposphere exchange (STE) flux (Gettelman et al., 1997; Hsu et al., 2005), counting the parcel trajectories with the TRAJ3D trajectory model (Langford et al.,

2012; Li et al., 2015), and tagging the stratospheric O_3 tracer with a chemical transport model (Lin et al., 2015; Wang et al., 2020; Zhang et al., 2022). Various approaches have been used to calculate the STE flux; however, their results still have large uncertainties, varying from 400 to 600 Tg/yr (Hsu et al., 2005; Stevenson et al., 2006). Hegglin and Shepherd (2009 also used a box model to calculate the STE flux and demonstrated that the peak O_3 flux occurred in spring during 1960–1970 and shifted toward late spring/early summer during 2090–2100. The three-dimensional trajectory model provides another method for investigating the motion of air masses by counting the trajectories of parcels (Langford et al., 2012; Li et al., 2015). They demonstrated that the trajectory model captured SI and contributed 3–6 ppbv to surface O_3. The tagging stratospheric air mass method is a more direct method for quantifying the impact of SI on tropospheric O_3. They estimated that the average contribution of SI was in the range of 1.5–10 ppb, which is closely related to altitude (Chang et al., 2023; Lin et al., 2015; Zhang et al., 2022). To the best of our knowledge, studies on the quantification of the contribution of SI have primarily focused on the Northeastern and mid-latitude regions in China, whereas the contributions of SI in Southeastern China have been less investigated.

Hong Kong, which is located in a subtropical region, has suffered from O_3 pollution during spring in recent years. Extensive studies have been conducted to elucidate the underlying mechanisms governing springtime O_3 pollution using model simulations and collaborative observations from O_3 sounding, surface samplers, and lidar remote sensing (Chan et al., 2000; Han et al., 2019; Jian and Fu, 2014; Zhao et al., 2021b). However, a consensus on the actual reasons for this is yet to be reached. Most studies claim that the long-range transport of biomass burning from Southeast Asia is responsible for the lower tropospheric O_3 enhancement over Hong Kong during springtime (Chan, 2017; Oltmans et al., 2004). Both O_3 and its precursor species can be transported to Hong Kong, thereby exacerbating surface O_3 pollution and activating photochemical reactions. In addition to the transport of biomass burning, a few studies have reported that SI also plays an indispensable role in determining the tropospheric

O_3 budget in Hong Kong (Zhao et al., 2020; Zhao et al., 2021a). However, the contribution of SI to surface O_3 in this region remains insufficiently investigated and inadequately quantified, although it is directly related to the effective implementation of the O_3 control strategy in Hong Kong.

In this study, to address the literature gap and provide insight into effective O_3 control strategies in Hong Kong, we applied a fully coupled "online" Weather Research and Forecasting model coupled with Chemistry (WRF-Chem) along with multiple datasets. This approach was used to quantify the impact of SI and explore an improved emission reduction path under the constraint of SI impact during a deep SI event. The objectives of this study were to 1) calculate the STE O_3 flux, (2) quantify the contribution of SI to tropospheric O_3, and (3) investigate an enhanced emission reduction pathway while considering the constraints imposed by the SI impact.

2. METHODS

2.1 WRF-Chem configurations

WRF-Chem (v3.9.1) is a widely used regional numerical meteorological model with a chemistry component developed by the US National Center for Atmospheric Research (NCAR) that is capable of reproducing meteorological variables and chemical species. Three nested domains are conducted in the simulation with grid points of 140×130, 130×118, and 118×106 from the outermost to the innermost domains, respectively. As shown in **Figure S1**, the outermost domain (D1) covers East Asia, Southeast Asia, and the northwestern Pacific with a grid spacing of 27 km, the middle domain (D2) covers most of the central and eastern regions of China with a spatial resolution of 9 km, and the innermost domain (D3) includes the Pearl River Delta with a resolution of 3 km. Vertically, 46 layers were set from the lowest vertical layer of 40 m to the 50-hPa level.

The initial and lateral boundary meteorological conditions were driven by the US

National Centers for Environmental Prediction Final Analysis data, with a horizontal resolution of 1°×1°. Land use data in the WRF model were provided by the Moderate Resolution Imaging Spectroradiometer. Anthropogenic emissions were generated based on the 2020 Multi-resolution Emission Inventory for China (http://www.meicmodel.org) with a $1^\circ \times 1^\circ$ resolution, published by Tsinghua University. The Model of Emissions of Gases and Aerosols from Nature was used to generate biogenic VOC emissions (Guenther et al., 2006). The initial chemical and lateral conditions were generated from the outputs of the Whole Atmosphere Community Climate Model (WACCM). In this study, the WRF-Chem simulation was driven by the Regional Acid Deposition Model Version 2 for gas-phase chemistry (Stockwell et al., 1990). The details of the model configurations are provided in the Supplementary Material (**Table S1**).

Owing to the lack of consideration of the stratospheric chemistry, current regional atmospheric chemistry models are unable to reproduce the dynamic process of transporting O_3 from the stratosphere to the troposphere, thus limiting the quantification of the impact of SI. To overcome this shortcoming, the upper boundary condition (UBC) scheme developed by Barth et al. (Barth et al., 2012) was applied to the simulation. The key chemical species (i.e., O_3, NO_x, nitric acid, methane, carbon monoxide, and nitrous oxide) are regulated by climatological means based on the outputs from the global atmospheric chemical model results between 50 hPa and the tropopause. When the UBC scheme is applied, the SI process is captured well by the WRF-Chem model (Chang et al., 2023; Zhao et al., 2021a).

2.2 WACCM dataset

The WACCM is a comprehensive chemistry–climate model developed by the NCAR. The meteorological fields of WACCM datasets are produced from the outputs of the NASA Global Modeling Assimilation Office Goddard Earth Observing System Model. Anthropogenic emissions are obtained from the latest Copernicus Atmosphere

Monitoring System inventory, and fire emissions are generated from the Fire INventory from NCAR v1 (Wiedinmyer et al., 2011). It has 88 vertical levels and a horizontal resolution of 0.9 latitude × 1.25 longitude. The stratospheric O_3 tracer (O_3S) is embedded into the WACCM, in which the stratospheric tracer is identical to the O_3 concentration above the tropopause, which is then removed at a tropospheric chemistry rate when it is transported into the troposphere. Stratospheric O_3 tagging is widely used to evaluate the stratospheric contribution (Chang et al., 2023; Ni et al., 2019).

2.4 SI O_3 flux calculation

To quantify the SI net O_3 flux, the box model approach developed by Appenzeller et al. (1996) was used in this study. Based on the continuity of the air mass, SI O_3 flux was calculated using the following equation:

$$F_{out} = F_{in} - \frac{dM}{dt} \quad (1)$$

where F_{in} represents the downward O_3 flux across the tropopause, calculated as the area-weighted integral of the hourly mean O_3 concentration multiplied by the negative hourly mean vertical velocity over Hong Kong. In this study, M denotes the total mass of O_3 contained in the lowermost stratosphere (defined as the region between the 100 hPa surface and 1 PVU), and dM/dt is the O_3 mass changes in a pre-defined region in one hour.

2.5 European Centre for Medium-Range Weather Forecasts Atmospheric Reanalysis Data

The fifth generation of the European Centre for Medium-Range Weather Forecasts Reanalysis v5 (ERA5) products provides another method for investigating SI characteristics. Hourly ERA5 products, such as vertical velocity, relative humidity, potential vorticity (PV), and O_3 concentration, with a horizontal resolution of 0.5° and 137 levels from the surface up to 80 km, were collected to calculate the SI O_3 flux,

diagnose SI occurrences, and evaluate the WRF-Chem model performance.

3. RESULTS

3.1 General characteristics of SI episode in March 2022

Figure 1 depicts a comparison of the retrieved ERA-5, WACCM, and WRF-Chem-simulated time cross-sections of O_3 averaged over Southern China during March 5–12, 2022.

Overall, the temporal and spatial distributions of O_3 simulated by WRF-Chem were in good agreement with the ERA5 and WACCM products, capturing two instances of stratospheric O_3 intrusion. A statistical evaluation of O_3, RH, wind speeds, and temperature is shown in **Table S2**. Overall, the model exhibited good performance of hourly O_3, RH, wind speeds, and temperature simulation, with a correlation coefficient (R) of 0.58-0.96. As highlighted by the white arrow in the WRF-Chem simulation, O_3-enriched air descends to 700 hPa but is then blocked and does not further intrude the surface layer. Conversely, the ERA5 and WACCM simulations revealed that the O_3-enriched air from the stratosphere further penetrated the boundary layer and persistently mixed with the surface layer over the following days.

As shown in **Figure 1**, a remarkable SI episode was observed in Southeastern China during March 7–8, 2022, which provided an opportunity to investigate the impact of SI on tropospheric O_3 pollution. A tongue-shaped plume with high O_3 concentrations extending from the stratosphere to the troposphere was observed on March 7. The magnitude of the O_3 mixing ratio centered on the intruded tongue reached 100 ppb, with high O_3 values (over 60 ppbv) extending to approximately 700 hPa. After the O_3 tongue-shaped plume reached 700 hPa, the strong downward motion further transported stratospheric O_3-rich air injected into the boundary layer, with O_3 reaching 60.0 ppbv on March 7–8. Accompanied by O_3-laden air intrusions, the downward transport of the high PV area agreed well with the O_3 distribution, providing evidence for a deep SI event penetrating the boundary layer level. One day later, the SI event concluded with

a strong downward air movement, transitioning to a weak upward motion. During March 10–12, a weak sinking flow transported a stratospheric air mass with relatively less O_3 at 70 ppbv downward to 500 hPa. Previous studies have demonstrated that SI intensity is closely related to variations in large-scale circulation (Chang et al., 2023; Jiang et al., 2015; Zhao et al., 2020; Zhao et al., 2021a).

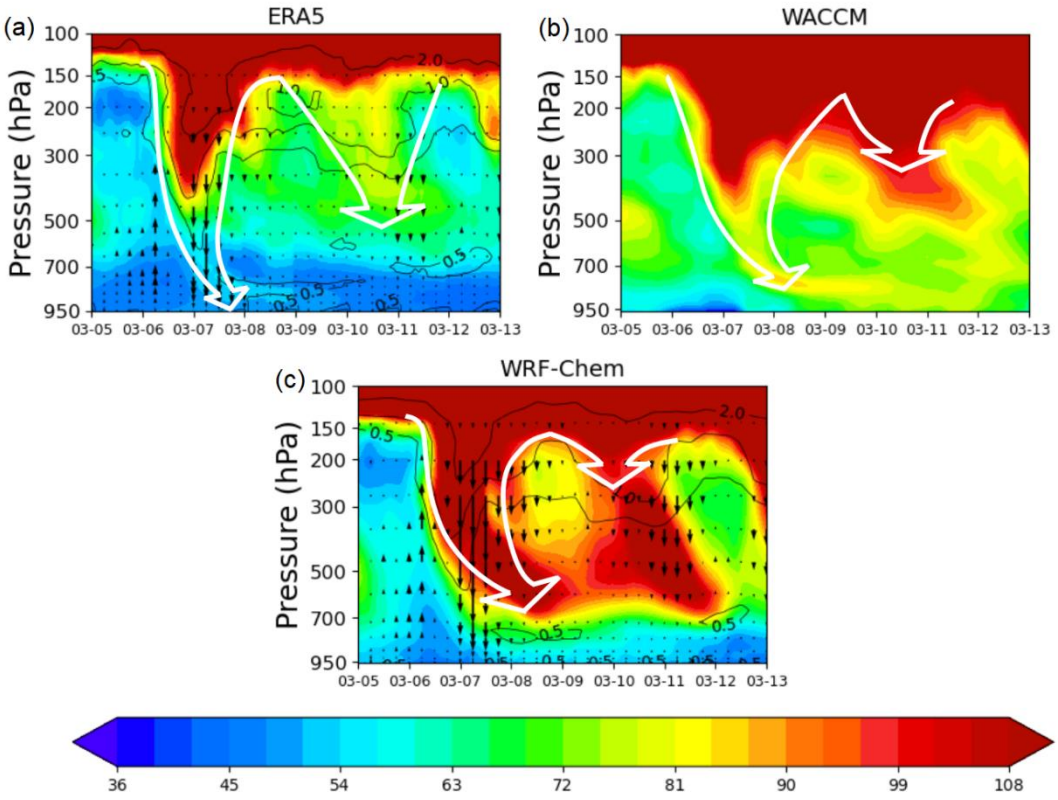

Figure 1. Temporal cross-section of O_3 (unit: ppb) averaged over the region (20°–35°N, 110°–118°E) during March 5–12, 2022. The black contour line indicates the dynamical tropopause of 1 PVU. The white arrow indicates the transport pathway of stratospheric O_3 into the troposphere.

Deep SI episodes are generally associated with favorable synoptic systems (Chang et al., 2023; Zhao et al., 2021a). On March 6, a cold front formed in northwestern Hong Kong (**Figure 2a**), leading to the development of maximum precipitation following the evolution of the maximum low-level convergence ahead of the cold front. Consequently, the upward air motion associated with the low-level convergence in Hong Kong was not conducive to the downward transport of stratospheric air from the free troposphere into the surface layer. One day later, as the cold front passed through Hong Kong, the interaction between the upper-level convergence and low-level divergence resulted in

a vertical downward motion, facilitating the descent of the O_3-laden air mass from the top of the atmospheric boundary layer (ABL). On March 8, a high-pressure system situated over the East China Sea influenced Hong Kong by subsiding air at the periphery of the system, leading to a vertical downward movement. By March 9, the center of the high-pressure system had shifted to the Korean Peninsula, gradually exerting control over Hong Kong. **Figure 3** further illustrates the cloud coverage (shaded area) and upper-level divergence in the 300-150 mb layers. During March 7–8, a distinct absence of cloud cover (darker area in the satellite imagery) and pronounced divergence were observed in the upper troposphere within 20°N–30°N and 110°E–120°E. These observations indicated the occurrence of a dry intrusion of air flowing from the lower stratosphere.

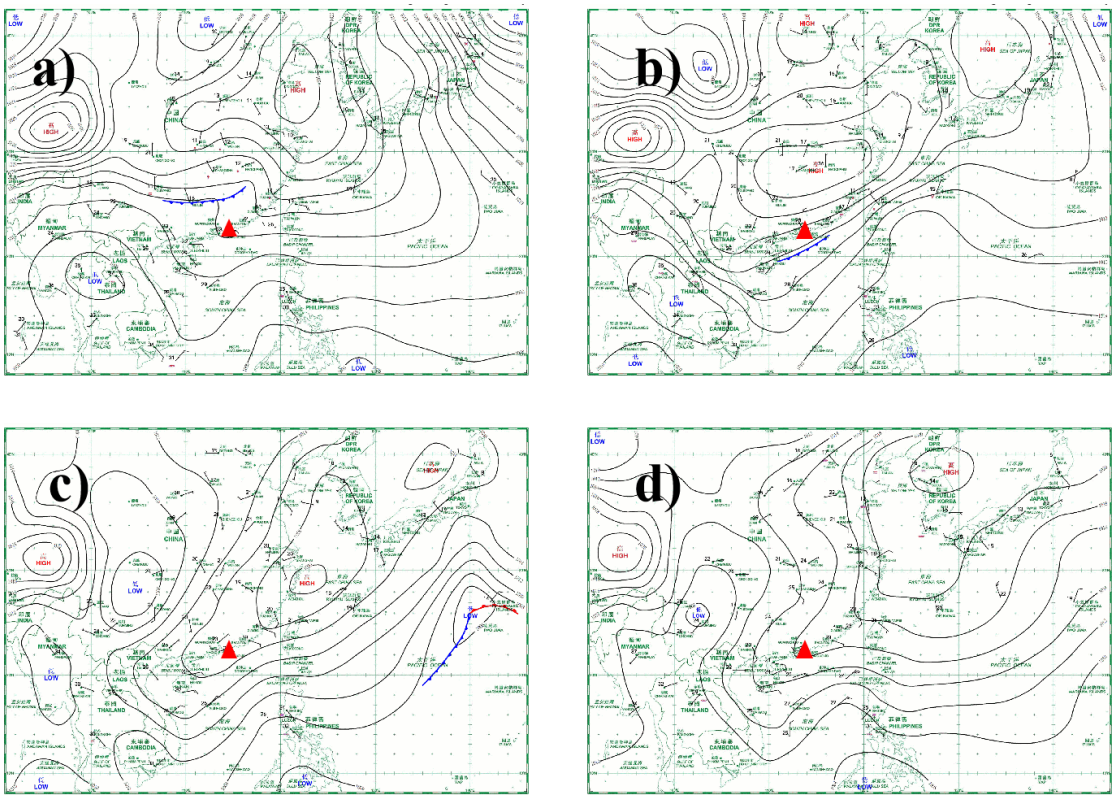

Figure 2. Surface weather charts provided by the Hong Kong Observatory for March 6–9, 2022. The red triangle indicates the location of Hong Kong.

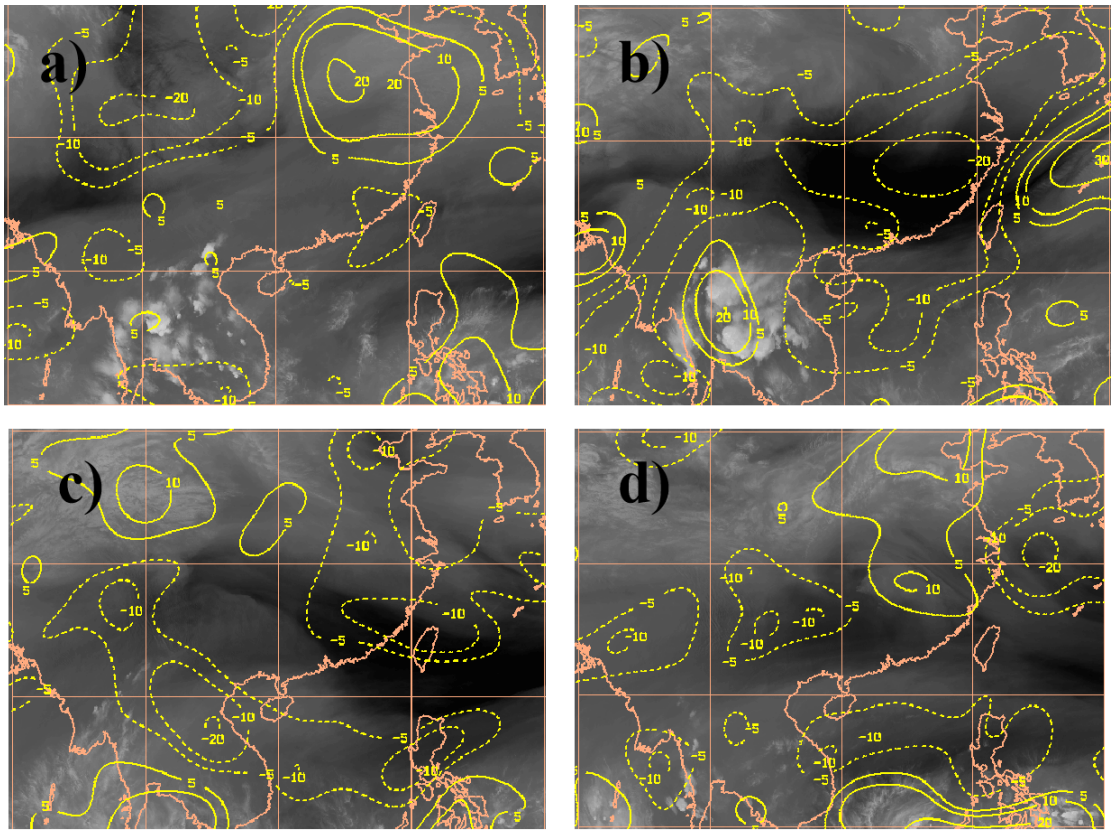

Figure 3. Japanese Geostationary Meteorological Satellite 5-retrieved cloud coverage (shaded area) and divergence (contour) at the 300–150 mb layers (provided by the Japan Meteorological Agency) at 1300 LST for March 6–9, 2023.

3.2 Quantification of the impact of SI on tropospheric O_3

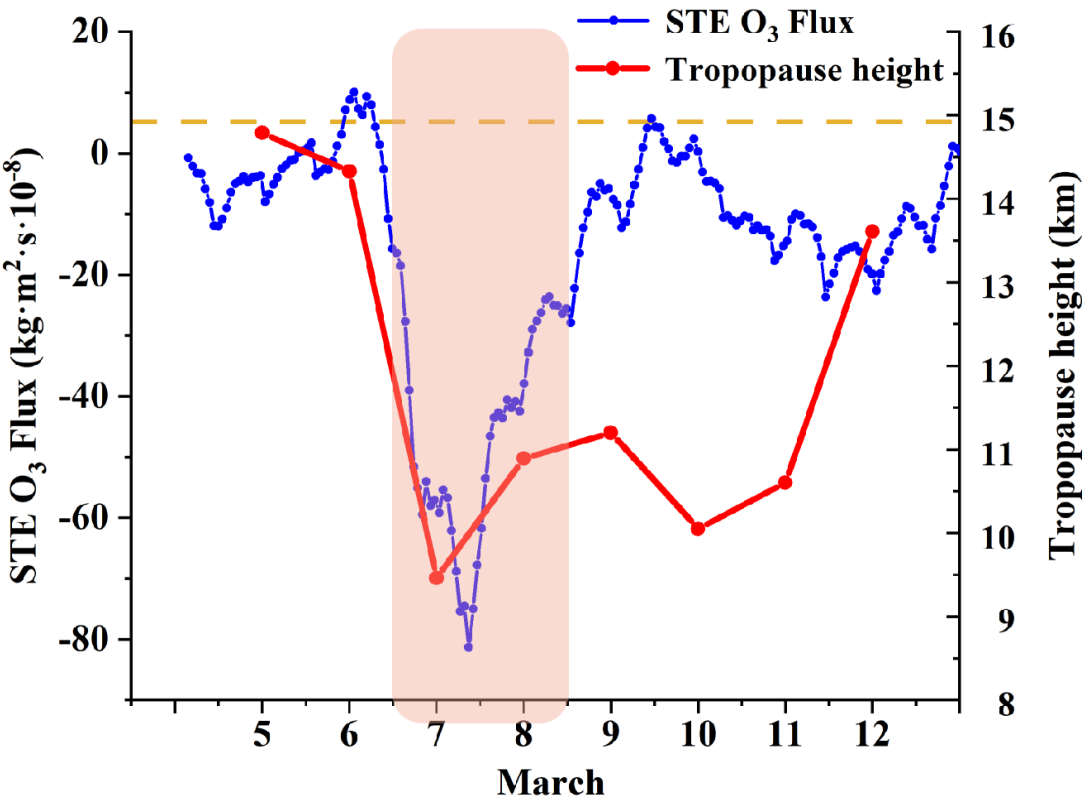

Figure 4. Hourly STE O_3 flux (blue solid line) and daily tropopause height (red solid line) during March 5–12, 2022 (yellow dashed line: monthly mean STE O_3 flux). The deep SI episodes are highlighted in the red areas.

Figure 4 depicts the time series of hourly STE O_3 fluxes across the tropopause from March 5 to 12. Tropopause height was determined using a PV threshold of 1 PVU. The hourly STE O_3 fluxes significantly increased from 9.37×10^{-8} kg·m^{-2}·s^{-1} on March 6 to -81.33×10^{-8} kg·m^{-2}·s^{-1} on March 7, which is 15.2-fold higher than the monthly mean O_3 flux of 5.7×10^{-8} kg·m^{-2}·s^{-1}. Strong negative STE O_3 fluxes were observed during the deep SI episode, suggesting the intrusion of stratospheric O_3-enriched air deeply into the troposphere. Associated with the strengthened O_3 flux, the tropopause height decreased rapidly from 14.3 km to 9.5 km. The close co-evolution of the STE O_3 flux and tropopause height provides convincing evidence for a deep SI event. After the SI episode, the STE O_3 flux returned to the monthly mean level with an increase in tropopause height. Overall, our findings revealed that the downward O_3 flux across the tropopause during this deep SI event was an order of magnitude greater than the

monthly mean average, potentially contributing substantially to tropospheric O_3 enhancement.

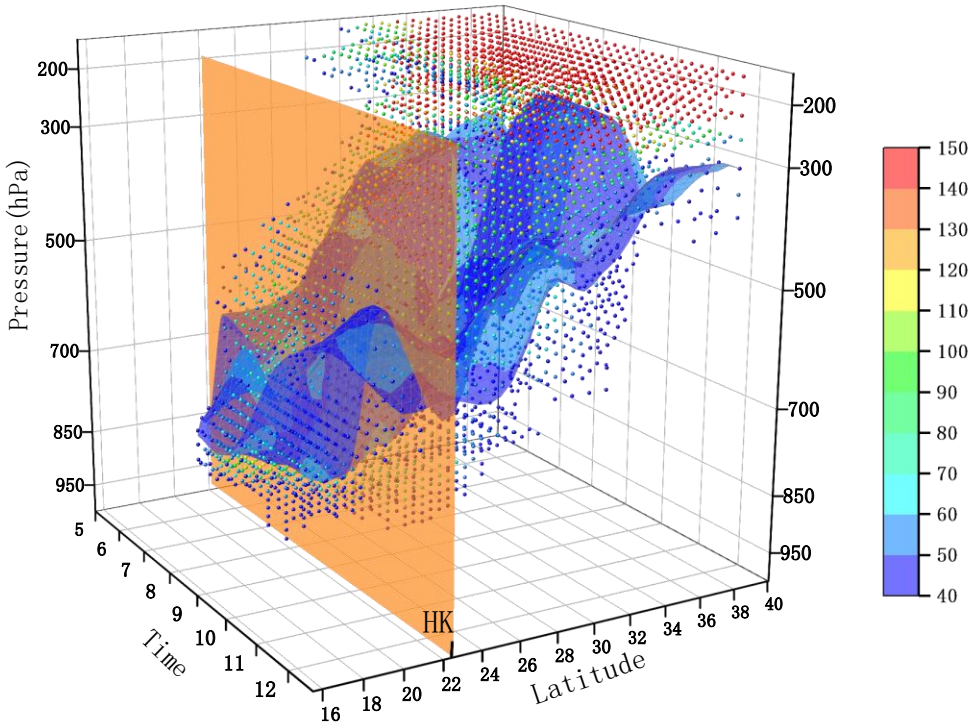

Figure 5. Three-dimensional structure of the stratospheric O_3 tracer transported to the surface, averaged along 114.2°E. The blue isosurface represents the pathway of O_3S at 50 ppbv. The location of Hong Kong is highlighted by the orange area.

To characterize the SI process, the three-dimensional structure of the stratospheric O_3 tracer during the deep SI episode is shown in **Figure 5**. O_3S plumes with concentrations exceeding 150 ppb were injected into the troposphere from the stratosphere at high latitudes. After crossing the tropopause, the O_3-enriched air extended from 200 hPa over the mid–high latitude region downward to Hong Kong at 700–800 hPa. A pool of high O_3S concentrations of up to 60 ppbv was observed over 20°N–24°N, indicating a non-negligible role of the contributions of SI in tropospheric O_3 enhancement. Upon reaching the lower troposphere in Hong Kong, the downward intrusion of the O_3 channel rapidly sets upright during March 7–8 within one day of downward transport to the surface layer. Influenced by the synoptic-scale deep SI following a north-to-south

transport pathway, O_3-enriched air transported to the ground may aggravate surface O_3 pollution. The contribution of SI to surface O_3 in Hong Kong was approximately 40 ppbv. During March 10–11, stratospheric O_3 with high momentum was blocked from penetrating the boundary layer, which had a limited impact on the surface O_3 budget.

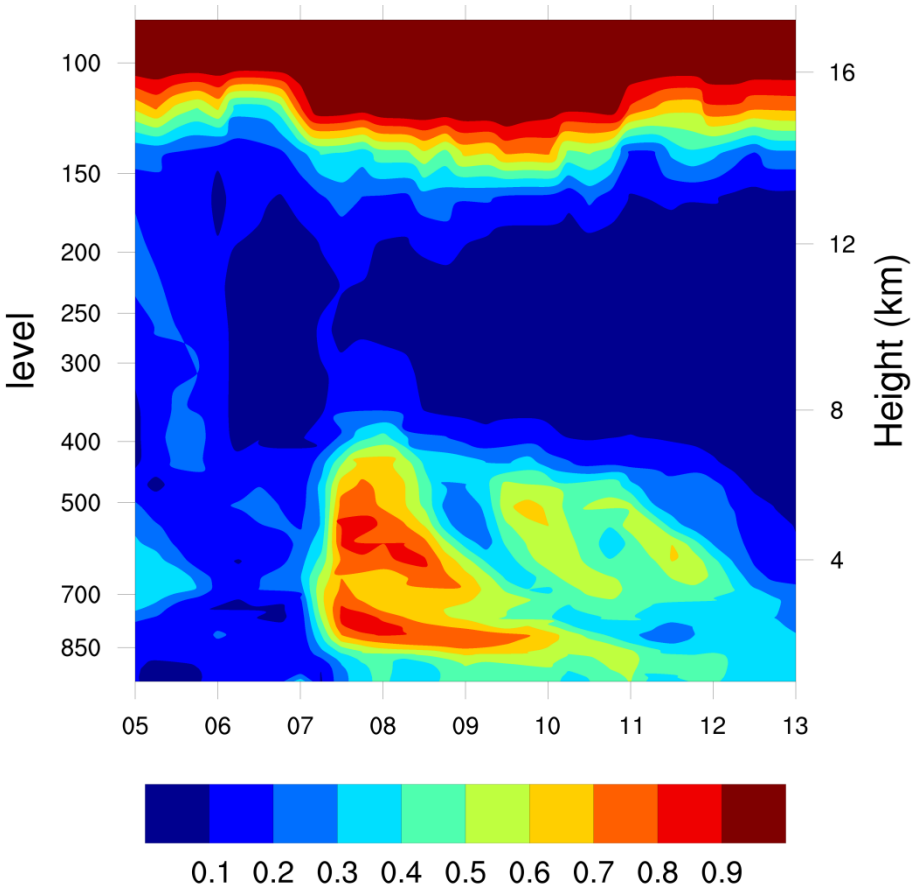

Figure 6. Temporal evolution of vertical distributions of the ratio of O_3S/O_3 in Hong Kong during March 5–12, 2022.

As discussed above, stratospheric air intruded from the upper level in the 30°N–40°N region and was transported downward to the lower troposphere in Hong Kong. Next, we quantified the contribution of SI to tropospheric O_3 in Hong Kong.

As observed in **Figure 6**, the center of the high stratospheric O_3 pool, with an O_3S to O_3 ratio larger than 0.7, appeared in the lower troposphere during March 7–8, which was transported from the mid–high latitude region. This O_3S pool contributed to an increase in surface O_3 concentrations through fumigation and vertical mixing in the

morning. One day later, the O_3S to O_3 ratio rapidly decreased to 0.2 due to the diminished SI process in the upstream region (**Figure 1**).

During March 10–12, a relatively weak SI event occurred in the mid–high latitude region, resulting in the transport of relatively limited stratospheric O_3 to the Hong Kong region. These inputs only account for 4%–8% of the O_3 in the middle troposphere. Owing to unfavorable meteorological conditions, stratospheric O_3 was blocked from entering the boundary layer. However, the accumulated O_3S during the previous deep SI event continuously mixed into the near ground, which could explain up to 40%–50% of the surface O_3.

In contrast to previous studies, the O_3 enhancement was not directly transported downward from the stratosphere along the upright column over Hong Kong (Chang et al., 2023; Wang et al., 2020). No SI events were observed in Hong Kong during the study period. Because the O_3S pool is disconnected from stratospheric O_3, lower tropospheric O_3 was misdiagnosed as a contributor to the long-range transport of biomass burning. Consequently, the contribution of biomass burning was excessively amplified, whereas the role of SI was underestimated. Our results highlight that stratospheric O_3 can still modulate the surface O_3 budget even though no SI was detected over Hong Kong and underscore the significance of characterizing the behaviors of SI in middle latitudes to gain insight into natural sources leading to O_3 pollution over subtropical regions.

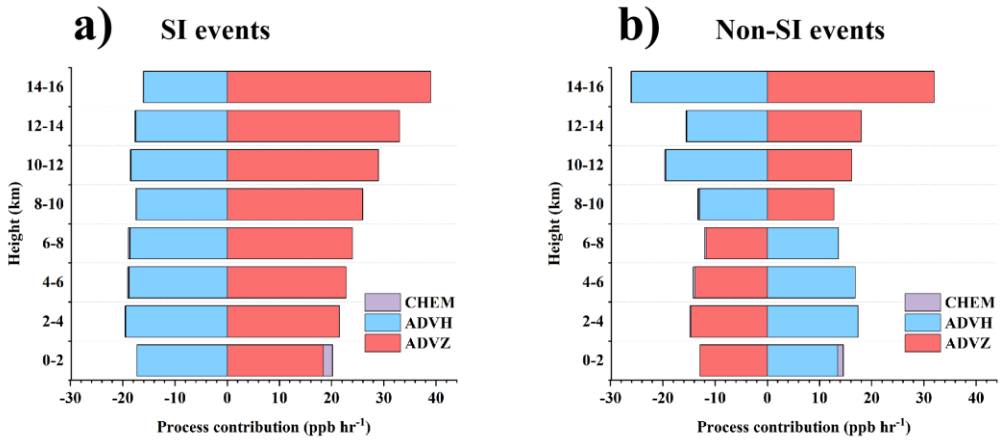

Figure 7. Contribution of individual process to O_3 changes during the (a) deep SI event and (b) non-SI events. (CHEM, chemical reaction; ADVH, horizontal advection; ADVZ, vertical advection)

To better understand the contributions of individual processes, the integrated process rate (IPR) approach was used to retrieve the horizontal advection, vertical advection, and chemical contributions to the O_3 increase during deep SI events (**Figure 7a**). We observed that, overall, vertical advection contributed predominantly to O_3 enhancement over the pre-defined region during the deep SI event. This contribution gradually decreased as the altitude decreased. The evident positive contribution from vertical transport was caused by the subsidence of air from the stratosphere downward to the surface layer with average contributions of 39 ppbv·hr^{-1} in 14–16 km and 18.4 ppbv·hr^{-1} below 2 km. Conversely, horizontal transport played a negative role in O_3 enhancement, with contributions ranging from −16.0 to −19.4 ppbv·hr^{-1}.

For comparison, the contributions of vertical and horizontal transport and chemical reactions to O_3 changes during non-SI events are depicted in **Figure 7b**. Through IPR analysis, the accumulated O_3 through vertical transport averaged in the range of 12.8 ppbv·hr^{-1}–32.0 ppbv·hr^{-1} between 8 km and 16 km, whereas it showed a negative contribution below 8 km. Notably, chemical reactions contributed 1.8 ppbv·hr^{-1} and 1.1 ppbv·hr^{-1} to the surface O_3 budget during the SI and non-SI events, respectively.

3.3 Contributions of SI to surface O_3

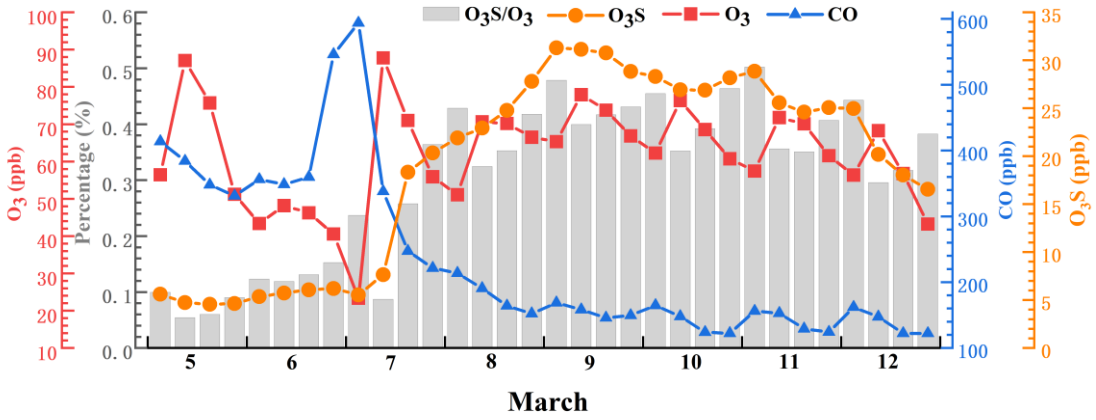

Figure 8. Time series of surface O_3 (red line), carbon monoxide (CO, blue line), stratospheric O_3 tracer (orange line), and the ratio of O_3S/O_3 (grey bar) from March 5 to 12, 2022, in Hong Kong.

As discussed above, SI transports O_3-enriched air downward to the lower free atmosphere, leading to substantial O_3 enhancement within the layers from the top of the ABL to a height of 3–4 km above ground level (**Figure 7**). We further restricted our focus to assessing the impact of SI on surface O_3 concentrations.

Previous studies have characterized SI as O_3-rich (Browning, 1997; Danielsen, 1968; Holton et al., 1995) with CO-poor (Fischer et al., 2000; Knowland et al., 2017) air, which increases the O_3S/O_3 ratio and dilutes the surface CO concentration. Therefore, we further investigated the co-evolution of O_3, O_3S, and CO in Hong Kong during the SI events. Before the stratospheric air mass reached the surface (i.e., March 5–6), the CO concentration was within the range of 331.3–546.2 ppbv, with averaged relative contributions of SI of approximately 6%–15%. During the deep SI period (March 7–8), the daily averaged O_3S level increased from 5.7 ppbv on March 6 to 13.0 ppbv on March 7 and further to 24.4 ppbv on March 8. In contrast, a significant decreasing trend in CO from 593.9 ppbv to 164.2 ppbv was observed, with corresponding ratios of O_3S/O_3 being 8.7% on March 7 and 41.8% on March 8. Following the continuous mixing of the accumulated stratospheric air mass into the surface layer (March 9–12), the

contribution of SI explained up to 50% of the surface O_3 budget associated with a more rapid decrease in surface CO, which was substantially reduced to 122.3 ppbv.

Overall, such an abnormal percentage of O_3S/O_3 and low CO level provided observational evidence for a deep SI event of O_3-enriched air originating in the stratosphere and penetrating the surface in Hong Kong, which may potentially affect the effectiveness of emission reduction strategies.

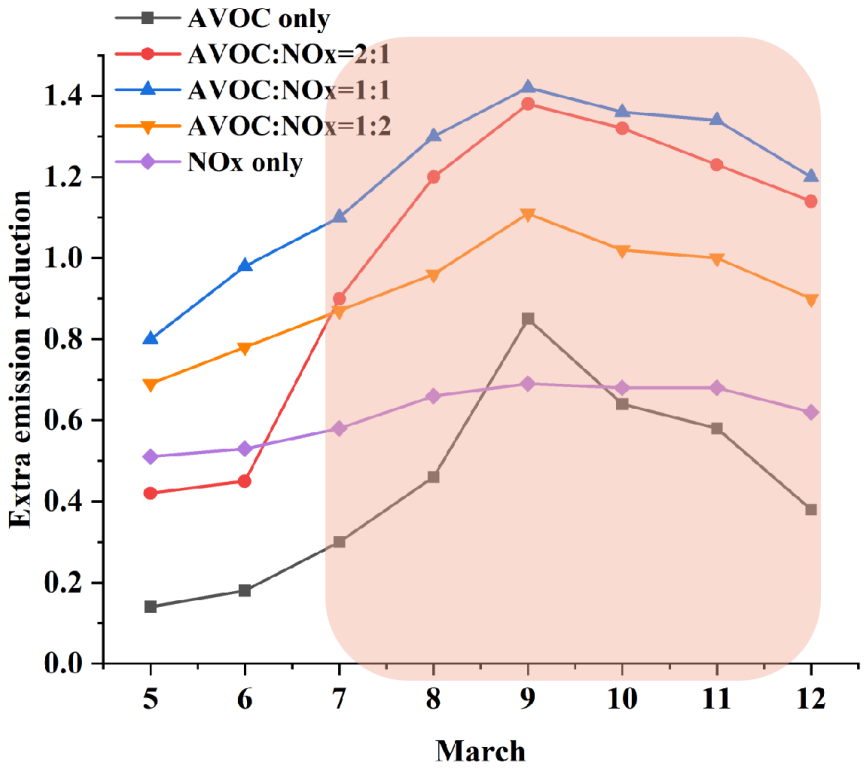

Figure 9. Extra emission reductions to offset the negative impact of SI following five different emission reduction paths in Hong Kong from March 5 to 12, 2022. The red shading highlights the period of stratospheric O_3 reaching the surface.

As discussed above, SI, the largest natural source of tropospheric O_3, exacerbates surface O_3 pollution, which may partly weaken the effectiveness of emission reduction strategies. To offset the negative contribution of SI, we conducted a set of sensitive simulations to obtain additional emission reductions in Hong Kong, following the five emission reduction paths.

As shown in **Figure 9**, different emission reduction pathways exhibited significant

differences in effectiveness when addressing the impact of stratospheric O_3 intrusion. Before the deep SI event, the extra emission reduction ratio was the lowest for the "AVOC only" reduction path, followed by the "AVOC/NO_x = 2:1," "NO_x only," "AVOC/NO_x = 1:2," and "AVOC/NO_x = 1:1" paths. During the deep SI event, the effective emission reduction path was re-ordered as the "AVOC only," "NO_x only," "AVOC/NO_x = 1:2," "AVOC/NO_x = 2:1," and "AVOC/NO_x = 1:1" paths. Within the five reduction paths considered, the "AVOC only" path showed the highest capacity to offset the contribution of SI, with approximately 14.0%–64.0% emissions reduction throughout the entire period, except for March 9. Considering that stratospheric O_3 reached its peak value on March 9, it is evident that the "NO_x only" reduction pathway holds a higher potential for offsetting the negative impact of stratospheric O_3 increase. In Hong Kong, the contribution of the stratospheric O_3 increase could be effectively mitigated by a 69.0% reduction in NOx emissions, surpassing the efficacy of an 85.0% reduction in AVOCs. In addition, equally reducing NO_x and VOC emissions might be the least efficient method for offsetting the negative contribution of SI when the total reduction ratio was within the range of 80%–142%.

Overall, additional anthropogenic emissions reductions must be conducted when O_3-enriched air is transported downward from the stratosphere and penetrates the surface. When the contribution of SIs is minimal, it is imperative to prioritize AVOC controls. Conversely, in cases where SIs have a significant impact, emphasis should be placed on NOx control.

4. DISCUSSION

China is currently facing severe O_3 pollution despite significant efforts to reduce anthropogenic emissions. Although substantial strides have been made in emission reduction initiatives, O_3 concentrations in major urban clusters have shown a troubling trend of increasing rather than decreasing. In addition to the complexities of the non-

linear relationships between O_3 and its precursors, a critical oversight in the formulation of reduction strategies is the impact of stratospheric O_3 intrusion into the troposphere. Failure to consider the influence of SI on ground-level O_3 concentrations hampers the effectiveness of control strategies.

In this study, a typical deep SI event from March 5 to 22, 2022, was investigated using WACCM, ERA-5 data, and the WRF-Chem model. Overall, the WRF-Chem model effectively captured stratospheric O_3 intruding into the troposphere through tropopause folding. However, compared to the ERA5 and WACCM data, the WRF-Chem model failed to reproduce the impact of SIs on surface O_3. Therefore, studying the influence of SIs on near-surface conditions using the WRF-Chem model has limitations. With the passage of a cold front and the influence of a high-pressure system, elevated concentrations of tongue-shaped O_3 coupled with high PV values extend downward from the stratosphere to the lower troposphere.

It is crucial to clarify that, unlike typical cases of SI, the SI event investigated in this study in Hong Kong did not occur as a local-scale vertical descent from the stratosphere to the lower troposphere. Instead, it involved a cross-latitudinal transport process from mid-latitude regions to lower-latitude areas. Stratospheric O_3 was injected into the troposphere through the tropopause folding process in mid-latitude regions and subsequently transported to the lower troposphere in lower-latitude areas. The results from the stratospheric O_3 tracer further confirmed that despite the absence of SI in the upper troposphere in the local Hong Kong region, elevated concentrations of stratospheric O_3 were still observed in the lower troposphere, extending downward to the near-surface layer. Our results underscore the significance of considering the influence of SI from upstream regions when formulating strategies for O_3 control. While addressing local impacts is essential, a comprehensive approach to developing O_3 control strategies and selecting monitoring protocols for SIs should incorporate an understanding of the effects of higher latitudes.

To quantify the intensity of the deep SI event, we calculated the STE O_3 flux. Our findings revealed that the STE flux reached a maximum of -81.33×10^{-8} $kg\cdot m^{-2}\cdot s^{-1}$, which was equivalent to 15.2-fold the monthly average STE flux. IPR analysis further indicated that vertical transport processes exhibited a positive contribution to O_3 levels from 16 km to the surface during SI events. The contribution from vertical transport diminished from 39 $ppbv\cdot hr^{-1}$ at 16 km to 18.4 $ppbv\cdot hr^{-1}$ below 2 km, whereas the horizontal processes played a negative role in O_3 production. In comparison, during non-SI periods, vertical transport exhibited positive contributions within the range of 8–16 km, whereas below 8 km, it had a negative impact. This suggests that their influence is relatively limited to the lower troposphere and near surface layer.

By performing stratospheric O_3 tagging, our research delved into the temporal and spatial distribution of stratospheric O_3 tracers, providing a comprehensive understanding of the temporal variability and regional impact of SI on O_3 concentrations. Our investigation highlights the impact of SIs on near-surface air quality, as stratospheric O_3 accumulated within the lower troposphere penetrated the boundary layer and reached the surface layer. SI contributed approximately 5.5–31.1 ppbv to ground-level O_3 concentrations, with the maximum contribution reaching up to 50%. Concurrently, as stratospheric air descends to the surface, there is a pronounced dilution effect on surface CO concentrations.

Although SI is an inevitable natural process, proactive measures are essential to prevent further exacerbation of O_3 pollution. This key strategy involves a substantial reduction in anthropogenic emissions to counteract the negative impacts of SI. Our sensitive simulations demonstrated that, except for March 9, the “AVOC only” path was the optimal emission reduction path. Emission reductions within the range of 14.0% to 64.0% in AVOCs were identified as capable of offsetting the adverse impacts of SI. Therefore, in circumstances where the contribution of SI is notably high, it is recommended to shift the focus of control strategies from the “AVOC only” path to the “NOx only” path.

Although this study only focused on investigating a SI event, our results have important implications for the prevention and control of O_3 pollution in the southern China. On one hand, when developing exceptional events rule for SI events, in addition to considering the local SI events, the contribution of stratospheric O_3 transport from mid- to high-latitudes to low-latitudes also needs to be taken into account. On the other hand, the significant exacerbation of near-surface O_3 concentration levels during this particular deep SI has led to changes in the optimal path for O_3 control.

This study aims to enhance the effectiveness of mitigation efforts in response to the challenges posed by the negative impacts of SI. Addressing China's current O_3 pollution crisis necessitates a comprehensive approach that acknowledges the complexities of O_3 generation and considers the impact of stratospheric O_3 intrusions. When focusing on reducing anthropogenic emissions, it is equally crucial to address and mitigate the adverse effects of SI on emission reduction strategies. Establishing clear criteria for the detection of SI and implementing adaptive measures within regulatory frameworks are essential steps toward achieving O_3 attainment.

Reference

Appenzeller, C., Holton, J.R., Rosenlof, K.H., 1996. Seasonal variation of mass transport across the tropopause. J. Geophys. Res-Atmos. 101, 15071-15078. https://doi.org/10.1029/96jd00821.

Barth, M.C., Lee, J., Hodzic, A., Pfister, G., Skamarock, W.C., Worden, J., et al., 2012. Thunderstorms and upper troposphere chemistry during the early stages of the 2006 North American Monsoon. Atmos. Chem. Phys. 12, 11003-11026. https://doi.org/10.5194/acp-12-11003-2012.

Brewer, A.W., 1949. Evidence for a world circulation provided by the measurements of helium and water vapour distribution in the stratosphere. Q. J. R. Meteorol. Soc. 75, 351-363. https://doi.org/10.1002/qj.49707532603.

Browning, K.A., 1997. The dry intrusion perspective of extra-tropical cyclone development. Meteorol. Appl. 4, 317-324. https://doi.org/10.1017/S1350482797000613.

Chan, K.L., 2017. Biomass burning sources and their contributions to the local air quality in Hong Kong. Sci. Total. Environ. 596, 212-221. https://doi.org/10.1016/j.scitotenv.2017.04.091.

Chan, L.Y., Chan, C.Y., Liu, H.Y., Christopher, S., Oltmans, S.J., Harris, J.M., 2000. A case study on the biomass burning in southeast Asia and enhancement of tropospheric ozone over Hong Kong. Geophys. Res. Lett. 27, 1479-1482. https://doi.org/10.1029/1999gl010855.

Chang, F.Y., Li, J.D., Li, N., Liao, H., 2023. Stratospheric intrusion may aggravate widespread ozone pollution through both vertical and horizontal advections in eastern China during summer. Front. Env. Sci-Switz. 10. https://doi.org/10.3389/fenvs.2022.1115746.

Danielsen, E.F., 1968. Stratospheric-Tropospheric Exchange Based on Radioactivity, Ozone and Potential Vorticity. J. Atmos. Sci. 25, 502-518. https://doi.org/10.1175/1520-0469(1968)025<0502:STEBOR>2.0.CO;2.

Dobson, G.M.B., Massey, H.S.W., 1956. Origin and distribution of the polyatomic molecules in the atmosphere. Proc. Math. Phys. Eng. Sci. 236, 187-193. https://doi.org/10.1098/rspa.1956.0127.

Fischer, H., Wienhold, F.G., Hoor, P., Bujok, O., Schiller, C., Siegmund, P., et al., 2000. Tracer correlations in the northern high latitude lowermost stratosphere: Influence of cross-tropopause mass exchange. Geophys. Res. Lett. 27, 97-100. https://doi.org/10.1029/1999GL010879.

Gettelman, A., Holton, J.R., Rosenlof, K.H., 1997. Mass fluxes of O-3, CH4, N2O and CF2Cl2 in the lower stratosphere calculated from observational data. J. Geophys. Res-Atmos. 102, 19149-19159. https://doi.org/10.1029/97jd01014.

Guenther, A., Karl, T., Harley, P., Wiedinmyer, C., Palmer, P.I., Geron, C., 2006. Estimates of global terrestrial isoprene emissions using MEGAN (Model of Emissions of Gases and Aerosols from Nature). Atmos. Chem. Phys. 6, 3181-3210. https://doi.org/10.5194/acp-6-3181-2006.

Han, H., Liu, J., Yuan, H.L., Wang, T.J., Zhuang, B.L., Zhang, X., 2019. Foreign influences on tropospheric ozone over East Asia through global atmospheric transport. Atmos. Chem. Phys. 19, 12495-12514. https://doi.org/10.5194/acp-19-12495-2019.

Hegglin, M.I., Shepherd, T.G., 2009. Large climate-induced changes in ultraviolet index and stratosphere-to-troposphere ozone flux. Nat. Geosci. 2, 687-691. https://doi.org/10.1038/ngeo604.

Holton, J.R., Haynes, P.H., Mcintyre, M.E., Douglass, A.R., Rood, R.B., Pfister, L., 1995. Stratosphere-Troposphere Exchange. Rev. Geophys. 33, 403-439. https://doi.org/10.1029/95rg02097.

Hsu, J., Prather, M.J., Wild, O., 2005. Diagnosing the stratosphere-to-troposphere flux of ozone in a chemistry transport model. J. Geophys. Res-Atmos. 110. https://doi.org/10.1029/2005jd006045.

Jian, Y., Fu, T.M., 2014. Injection heights of springtime biomass-burning plumes over peninsular Southeast Asia and their impacts on long-range pollutant transport. Atmos. Chem. Phys. 14, 3977-3989. https://doi.org/10.5194/acp-14-3977-2014.

Jiang, Y.C., Zhao, T.L., Liu, J., Xu, X.D., Tan, C.H., Cheng, X.H., et al., 2015. Why does surface ozone peak before a typhoon landing in southeast China? Atmos. Chem. Phys. 15, 13331-13338. https://doi.org/10.5194/acp-15-13331-2015.

Knowland, K.E., Ott, L.E., Duncan, B.N., Wargan, K., 2017. Stratospheric Intrusion-Influenced Ozone Air Quality Exceedances Investigated in the NASA MERRA-2 Reanalysis. Geophys. Res. Lett. 44, 10691-10701. https://doi.org/10.1002/2017gl074532.

Lachmy, O., Harnik, N., 2014. The Transition to a Subtropical Jet Regime and Its Maintenance. J. Atmos. Sci. 71, 1389-1409. https://doi.org/10.1175/Jas-D-13-0125.1.

Langford, A.O., 1999. Stratosphere-troposphere exchange at the subtropical jet: contribution to the tropospheric ozone budget at midlatitudes. Geophys. Res. Lett. 26, 2449-2452. https://doi.org/10.1029/1999gl900556.

Langford, A.O., Brioude, J., Cooper, O.R., Senff, C.J., Alvarez, R.J., Hardesty, R.M., et al., 2012. Stratospheric influence on surface ozone in the Los Angeles area during late spring and early summer of 2010. J. Geophys. Res-Atmos. 117. https://doi.org/10.1029/2011jd016766.

Li, D., Bian, J.C., Fan, Q.J., 2015. A deep stratospheric intrusion associated with an intense cut-off low event over East Asia. Sci. China. Earth. Sci. 58, 116-128. https://doi.org/10.1007/s11430-014-4977-2.

Lin, M.Y., Fiore, A.M., Horowitz, L.W., Langford, A.O., Oltmans, S.J., Tarasick, D., et al., 2015. Climate variability modulates western US ozone air quality in spring via deep stratospheric intrusions. Nat. Commun. 6. https://doi.org/10.1038/ncomms8105.

Ni, Z.Z., Luo, K., Gao, X., Gao, Y., Fan, J.R., Fu, J.S., et al., 2019. Exploring the stratospheric source of ozone pollution over China during the 2016 Group of Twenty summit. Atmos. Pollut. Res. 10, 1267-1275. https://doi.org/10.1016/j.apr.2019.02.010.

Olsen, M.A., Gallus, W.A., Stanford, J.L., Brown, J.M., 2000. Fine-scale comparison of TOMS total ozone data with model analysis of an intense Midwestern cyclone. J. Geophys. Res-Atmos. 105, 20487-20495. https://doi.org/10.1029/2000jd900205.

Oltmans, S.J., Johnson, B.J., Harris, J.M., Thompson, A.M., Liu, H.Y., Chan, C.Y., et al., 2004. Tropospheric ozone over the North Pacific from ozonesonde observations. J. Geophys. Res-Atmos. 109. https://doi.org/10.1029/2003jd003466.

Price, J.D., Vaughan, G., 1993. The Potential for Stratosphere Troposphere Exchange in Cut-Off-Low Systems. Q. J. R. Meteorol. Soc. 119, 343-365. https://doi.org/10.1002/qj.49711951007.

Stevenson, D.S., Dentener, F.J., Schultz, M.G., Ellingsen, K., van Noije, T.P.C., Wild, O., et al., 2006. Multimodel ensemble simulations of present-day and near-future tropospheric ozone. J. Geophys. Res-Atmos. 111. https://doi.org/10.1029/2005jd006338.

Stockwell, W.R., Middleton, P., Chang, J.S., Tang, X., 1990. The second generation regional acid deposition model chemical mechanism for regional air quality modeling. J. Geophys. Res-Atmos. 95, 16343-16367. https://doi.org/10.1029/JD095iD10p16343.

Stohl, A., Bonasoni, P., Cristofanelli, P., Collins, W., Feichter, J., Frank, A., et al., 2003. Stratosphere-troposphere exchange:: A review, and what we have learned from STACCATO -: art. no. 8516. J. Geophys. Res-Atmos. 108. https://doi.org/10.1029/2002jd002490.

Wang, H.Y., Wang, W., Huang, X., Ding, A.J., 2020. Impacts of stratosphere-to-troposphere-transport on summertime surface ozone over eastern China. Sci. Bull. 65, 276-279. https://doi.org/10.1016/j.scib.2019.11.017.

Westervelt, D.M., Ma, C.T., He, M.Z., Fiore, A.M., Kinney, P.L., Kioumourtzoglou, M.A., et al., 2019. Mid-21st century ozone air quality and health burden in China under emissions scenarios and climate change. Environ. Res. Lett. 14. https://doi.org/10.1088/1748-9326/ab260b.

Wiedinmyer, C., Akagi, S.K., Yokelson, R.J., Emmons, L.K., Al-Saadi, J.A., Orlando, J.J., et al., 2011. The Fire INventory from NCAR (FINN): a high resolution global model to estimate the emissions from open burning. Geosci. Model. Dev. 4, 625-641. https://doi.org/10.5194/gmd-4-625-2011.

Zhang, Y.J., Li, J., Yang, W.Y., Du, H.Y., Tang, X., Ye, Q., et al., 2022. Influences of stratospheric intrusions to high summer surface ozone over a heavily industrialized region in northern China. Environ. Res. Lett. 17. https://doi.org/10.1088/1748-9326/ac8b24.

Zhao, K.H., Hu, C., Yuan, Z.B., Xu, D.N., Zhang, S., Luo, H.H., et al., 2020. A modeling study of the impact of stratospheric intrusion on ozone enhancement in the lower troposphere over the Hong Kong regions, China. Atmos. Res. 247. https://doi.org/10.1016/j.atmosres.2020.105158.

Zhao, K.H., Huang, J.P., Wu, Y.H., Yuan, Z.B., Wang, Y.W., Li, Y., et al., 2021a. Impact of Stratospheric Intrusions on Ozone Enhancement in the Lower Troposphere and Implication to Air Quality in Hong Kong and Other South China Regions. J. Geophys. Res-Atmos. 126. https://doi.org/10.1029/2020JD033955.

Zhao, K.H., Luo, H.H., Yuan, Z.B., Xu, D.N., Du, Y., Zhang, S., et al., 2021b. Identification of close relationship between atmospheric oxidation and ozone formation regimes in a photochemically active region. J. Environ. Sci. 102, 373-383. https://doi.org/10.1016/j.jes.2020.09.038.

Zhao, K.H., Wu, Y.H., Yuan, Z.B., Huang, J.P., Liu, X.H., Ma, W., et al., 2022. Understanding the underlying mechanisms governing the linkage between atmospheric oxidative capacity and ozone precursor sensitivity in the Yangtze River Delta, China: A multi-tool ensemble analysis. Environ. Int. 160. https://doi.org/10.1016/j.envint.2021.107060.

CRediT authorship contribution statement

Kaihui Zhao: Methodology, Investigation, Software, Validation, Formal analysis, Writing - original draft. **Yuheng Chen:** Supervision, Validation, Formal analysis, Writing - review & editing. **Puyu Lian:** Supervision, Conceptualization, Methodology, Writing - review & editing. **Wenguang Li:** Software, Validation. **Fangyuan Yang:** Methodology, Validation. **Xiufang Zhang:** Formal analysis, Writing - review & editing. **Ruowen Yang:** Methodology, Writing - review & editing.

Acknowledgments

This study is supported by the National Natural Science Foundation of China (No. 42105164), Guangdong Basic and Applied Basic Research Foundation (No. 2022A1515011078), Xianyang key research and development program (No. L2022ZDYFSF040).

Competing interests

The authors declare no competing interests.

Data availability

The stratospheric O_3 tracer is retrieved from the NCAR (https://www2.acom.ucar.edu/gcm/waccm). The meteorological data are available from fifth generation ECMWF atmospheric reanalysis of the global climate (https://www.ecmwf.int/en/forecasts/dataset/ecmwf-reanalysis-v5). The Surface weather charts are provided by the Hong Kong Observatory (http://envf.ust.hk/dataview/hko_wc/current/). The WRF-Chem simulations in this study are available from the corresponding authors upon reasonable request.